

This is the accepted author manuscript of the publication

Combined PET imaging of the inflammatory tumor microenvironment identifies margins of unique radiotracer uptake.

Zinnhardt B¹, Pigeon H², Thézé B², Viel T³, Wachsmuth L⁴, Fricke IB³, Schelhaas S³, Honold L³, Schwegmann K³, Wagner S⁵, Faust A³, Faber C⁶, Kuhlmann MT³, Hermann S³, Schäfers M³, Winkeler A⁷, Jacobs AH³.

1 European Institute for Molecular Imaging, University of Münster
zinnhardt@wwu.de.

2 Imagerie Moléculaire In Vivo, Service Hospitalier Frédéric Joliot, Inserm, CEA, Univ. Paris Sud, CNRS, Université Paris Saclay, CEA.

3 European Institute for Molecular Imaging, University of Münster.

4 Department of Clinical Radiology, University of Münster.

5 Department of Nuclear Medicine, University Hospital Münster.

6 Department of Clinical Radiology, University Hospital Münster.

7 I2BM, Service Hospitalier Frédéric Joliot, CEA.

Published in **Cancer Research**

DOI: 10.1158/0008-5472.CAN-16-2628

First published online 31 Jan 2017

The final publication is available at

<http://cancerres.aacrjournals.org/content/early/2017/01/31/0008-5472.CAN-16-2628.long>

1 **Combined PET imaging of the inflammatory tumor microenvironment identifies margins of**
2 **unique radiotracer uptake**

3 *Running title: Imaging the glioma micro environment*

4 *Keywords: [¹⁸F]DPA-714, [¹⁸F]BR-351, [¹⁸F]FET, GAM, MMPs*

5
6 *Bastian Zinnhardt¹, Hayet Pigeon², Benoit Thézé², Thomas Viel^{1,3}, Lydia Wachsmuth⁴, Inga Berit Fricke¹,*
7 *Sonja Schelhaas¹, Lisa Honold¹, Katrin Schwegmann¹, Stefan Wagner⁶, Andreas Faust¹, Cornelius Faber^{4,5},*
8 *Michael T. Kuhlmann¹, Sven Hermann^{1,5}, Michael Schäfers^{1,5,6}, Alexandra Winkeler², Andreas H. Jacobs^{1,5,7}*

9 ⁽¹⁾ European Institute for Molecular Imaging (EIMI), Westfälische Wilhelms-University Münster,
10 Münster, Germany

11 ⁽²⁾ Imagerie Moléculaire In Vivo, Inserm, CEA, Univ. Paris Sud, CNRS, Université Paris Saclay, CEA -
12 Service Hospitalier Frédéric Joliot, Orsay, France

13 ⁽³⁾ PARCC INSERM-U970, Université Paris Descartes, Paris, France

14 ⁽⁴⁾ Department of Clinical Radiology, University Hospital Münster, Germany

15 ⁽⁵⁾ DFG EXC 1003 Cluster of Excellence 'Cells in Motion', University of Münster, Münster, Germany

16 ⁽⁶⁾ Department of Nuclear Medicine, University Hospital Münster, Germany

17 ⁽⁷⁾ Department of Geriatrics, Johanniter Hospital, Evangelische Kliniken, Bonn, Germany

18 ***Correspondence:** Prof. Andreas H. Jacobs, MD
19 European Institute for Molecular Imaging (EIMI), University of Münster
20 Waldeyerstr. 15, D-48149 Münster
21 Tel. +49 251 83 49300
22 Fax. +49 251 83 49313
23 ahjacobs@uni-muenster.de

24 **Conflict of interest**

25 The authors report no conflicting interests.

1 **Funding**

2 This research was partly funded by a fellowship of the 'Cells-in-Motion' Cluster of Excellence (DFG EXC
3 1003 - CiM) Graduate School, and the International Max-Planck Research School - Molecular Biomedicine
4 (IMPRS-MBM) Joint Graduate Program' to B. Zinnhardt, the EU 7th Framework Programme (FP7/2007-
5 2013) under grant agreement n° 278850 (INMiND), and by IZKF core unit PIX, Münster, Germany.

6

7

1

2 **Abstract**

3 The tumor microenvironment is highly heterogeneous. For gliomas, the tumor-associated inflammatory
4 response is pivotal to support growth and invasion. Factors of glioma growth, inflammation, and
5 invasion, such as the translocator protein (TSPO) and matrix metalloproteinases (MMP), may serve as
6 specific imaging biomarkers of the glioma microenvironment. In this study, non-invasive imaging by
7 positron emission tomography (PET) with [¹⁸F]DPA-714 (TSPO) and [¹⁸F]BR-351 (MMP) was used for
8 assessment of localization and quantification of the expression of TSPO and MMP. Imaging was
9 performed in addition to established clinical imaging biomarker of active tumor volume ([¹⁸F]FET) in
10 conjunction with magnetic resonance imaging (MRI). We hypothesized that each imaging biomarker
11 revealed distinct areas of the heterogeneous glioma tissue in a mouse model of human glioma. Tracers
12 were found to be increased 1.4-1.7 fold with [¹⁸F]FET showing the biggest volume as depicted by a
13 thresholding-based, volumes of interest (VOI) analysis. Tumor areas, which could not be detected by a
14 single tracer and/or MRI parameter alone, were measured. Specific compartments of [¹⁸F]DPA-714 (14%)
15 and [¹⁸F]BR-351 (11%) volumes along the tumor rim could be identified. [¹⁸F]DPA-714 (TSPO) and [¹⁸F]BR-
16 351 (MMPs) matched with histology. Glioma-associated microglia/macrophages (GAM) were identified
17 as TSPO and MMP sources. Multi-tracer and multi-modal molecular imaging approaches may allow us to
18 gain important insights into glioma-associated inflammation (GAM, MMP). Moreover, this non-invasive
19 technique enables characterization of the glioma microenvironment with respect to the disease-driving
20 cellular compartments at the various disease stages.

1

2 **Introduction**

3 Gliomas are highly dynamic, complex and heterogeneous tissues in which cancer cells themselves
4 stimulate their proliferation, neoangiogenesis and immune escape to serve their microenvironment(1).

5 In particular, tumor-associated inflammation has been linked to angiogenesis, metastatic potential, and
6 poor prognosis in patients(2). An abundant number of microglia/macrophages are recruited into the

7 tumor, and growing evidence demonstrates that glioma-associated microglia/macrophages (GAMs)

8 contribute to glioma growth and invasion, angiogenesis, and immune suppression and represent a

9 pivotal target for therapy(1,3). In order to better understand the role of glioma-associated inflammation

10 on tumor progression and to follow its impact during treatment, new imaging approaches are crucial to

11 characterize the inflammatory component of the tumor microenvironment. This is even more important

12 in view of new therapeutic approaches for glioma treatment, requiring imaging approaches to allow non-

13 invasive assessment of treatment efficacy and follow-up, as well as detection of a potential therapy-

14 induced switch from a proliferative to an invasive glioma phenotype(4).

15 Most glioma cells express the 18kDa translocator protein TSPO. Different studies demonstrated a

16 positive correlation between TSPO expression and grade of malignancy and a negative correlation with

17 survival(5,6). Within the heterogeneous glioma tissue, different cell types, neoplastic cells, GAMs and

18 astrocytes also express TSPO (7,8). Among the current (pre-)clinical positron emission tomography (PET)

19 tracers targeting TSPO, the second generation tracer, *N,N*-diethyl-2-(2-(4-(2-[¹⁸F]fluoroethoxy)phenyl)-

20 5,7-dimethylpyrazolo[1,5-a]pyrimidin-3-yl)acetamide ([¹⁸F]DPA-714) has been validated in several

21 models of glioma(7–9) and other neurological diseases(10,11). Besides being an excellent marker for

22 glioma growth and infiltration, [¹⁸F]DPA-714 has shown promise for the detection of glioma-associated

23 microglial activation(8,12).

1 Another target for imaging of gliomas are matrix metalloproteinases (MMPs). MMPs have been linked to
2 increased cell proliferation, tumor invasion, migration and poor prognosis in glioma patients(5,13,14).
3 Moreover, MMPs facilitate microglia-mediated glioma invasion(15), as for example invasion of glioma
4 cells is reduced in cultured brain slices in the absence of microglia cells(16) or promoted through the
5 increase of MMP-2 expression and activity(17). Besides that MMPs affect the neuroinflammatory milieu
6 by modulating the expression and activity of chemokines, inflammatory cytokines, growth factors,
7 receptor turnover and by affecting cellular migration(18).

8 For imaging of activated MMPs, the radiofluorinated MMP inhibitor (*R*)-2-(*N*-benzyl-4-(2-
9 [¹⁸F]fluoroethoxy)phenylsulphonamido)-*N*-hydroxy-3-methylbutanamide ([¹⁸F]BR-351), a derivative of
10 CGS 25966, has successfully been used for PET imaging of microglia-derived MMPs in a model of
11 ischemic stroke(10). [¹⁸F]BR-351 effectively binds to the activated forms of MMP-2, -8, -9, and -13,
12 whereas the latent forms of MMPs are not recognized(19).

13 Here, we used non-invasive PET imaging of TSPO and MMPs in a mouse model of human orthotopic
14 glioma aiming at detecting specific molecular patterns of glioma pathogenesis *in vivo*. Tumor growth,
15 tumor associated microglial activation, and MMP activation were studied and related to MRI and PET
16 together with *O*-(2-[¹⁸F]fluoroethyl)-*L*-tyrosine ([¹⁸F]FET)(20) as the clinical imaging biomarker for
17 assessing glioma extent. The aim of the present study was to investigate the combined use of [¹⁸F]DPA-
18 714 and [¹⁸F]BR-351 as new PET imaging biomarkers of tumor cell signals and the tumor
19 microenvironment. The hypothesis of the study was that each imaging biomarker reveals distinct areas
20 of glioma activity within the heterogeneous glioma tissue.

1

2 **Material and Methods**

3 ***Study design***

4 A multi-tracer, multi-modality approach was used to investigate the feasibility to image TSPO and active
5 MMPs in relation to tumor growth in a mouse model of human glioma.

6 All experiments were conducted in accordance with the German Law on the Care and Use of Laboratory
7 Animals and approved by the Landesamt für Natur, Umwelt und Verbraucherschutz of North Rhine-
8 Westphalia and the ARRIVE guidelines (<https://www.nc3rs.org.uk/arrive-guidelines>) (21).

9 Female NMRI nu/nu mice (Janvier, France), 8-11 weeks old, were housed at constant temperature (23°C)
10 and relative humidity (40 %) under a regular light/dark schedule. Food and water were available *ad*
11 *libitum*.

12 In total, $n=27$ mice were orthotopically (intra-striatal injection, coordinates in relation to bregma: lateral
13 -2.0 mm, anterior-posterior +0.5 mm, dorsal-ventral -3.0 mm) implanted with 2×10^5 human Gli36dEGFR-
14 LITG cells in 2 μ l PBS. As controls, sham animals ($n=6$) were injected with 2 μ l of PBS only. During
15 anesthesia, body temperature was maintained at physiological level with a custom built heating pad.
16 Mice were imaged 12-14 days after orthotopic implantation of glioma cells. First, T2-weighted (T2w) MRI
17 was conducted at day 12 post-implantation, followed by PET acquisition with [^{18}F]DPA-714 on the same
18 day and [^{18}F]BR-351, and [^{18}F]FET on consecutive days (days 13 and 14, respectively; *Sequence 1*).

19 A subgroup of mice ($n=4$) was imaged first with T2w MRI and [^{18}F]FET on the same day, followed by
20 [^{18}F]BR-351 and [^{18}F]DPA-714 on consecutive days (*Sequence 2*) (**Suppl. Fig. 1**). All imaging experiments
21 were performed within 48 h.

22 [^{18}F]DPA-714, [^{18}F]BR-351, and [^{18}F]FET PET, as well as T2w MR imaging data were available in the same
23 animal. All mice with successful multi-modal imaging were included in the data ($n=20$).

1 **Cell culture**

2 Gli36dEGFR glioma cells were obtained from Dr. David Louis (Molecular Neurooncology Laboratory,
3 MGH, Boston, MA)(22,23). Glioma cells were carefully cultured and observed. Tumor cells displayed
4 typical growth patterns and phenotypes *in vitro* and *in vivo*. The cells were not further genetically
5 authenticated. Cells were cultured as adherent monolayer in Dulbecco's Modified Eagle Medium (life
6 technologies, Darmstadt, Germany) with high glucose and GlutaMAX (Gibco) supplemented with 10%
7 Fetal Bovine Serum (Invitrogen), and 1% Penicillin/Streptomycin (PAA Laboratories) at 37°C in a 5%
8 CO₂/95% air atmosphere.

9 **Radiochemistry**

10 [¹⁸F]DPA-714 was prepared following the procedure described in the literature with a radiochemical
11 purity of 99 % and a decay corrected radiochemical yield (rcy) of 17.7 ± 8 %(24). The synthesis and
12 quality control of [¹⁸F]BR-351 was performed as described previously(19). [¹⁸F]BR-351 had a
13 radiochemical purity of 95.5% and a rcy of 7.0 ± 3.4 % due to a small impurity that could not be
14 separated during the last HPLC purification step. [¹⁸F]FET was prepared as described previously with a
15 radiochemical purity of 99% and rcy of 23.9 ± 4.3%(25). [¹⁸F]DPA-714, [¹⁸F]FET and [¹⁸F]BR-351 were
16 formulated in saline/EtOH 17/3 (v/v), water for injection/citrate-puffer/EtOH 19/4/1 (v/v/v) and
17 saline/EtOH 9/1 (v/v), respectively.

18 **PET studies**

19 During all experimental procedures, mice were anesthetized with 1.5-2 % isoflurane (Abbott Animal
20 Health, Illinois, USA) in 100% O₂. Mice were subjected to PET imaging using the radiotracers [¹⁸F]DPA-
21 714, [¹⁸F]BR-351, and [¹⁸F]FET for assessment of TSPO expression, MMP activity, and amino acid
22 transport, respectively. PET images were acquired on a high resolution small animal PET scanner (32
23 module quadHIDAC, Oxford Positron Systems Ltd., Oxford, U.K.) with uniform spatial resolution (<1 mm
24 FWHM). PET data were reconstructed using one-pass list mode expectation maximization algorithm with

1 resolution recovery(26). [¹⁸F]DPA-714 PET images were acquired 45-75 min post i.v. injection of $17.7 \pm$
2 2.6 MBq [¹⁸F]DPA-714. [¹⁸F]BR-351 PET images were acquired 95-110 min post i.v. injection of 22.4 ± 2.7
3 MBq [¹⁸F]BR-351. [¹⁸F]FET PET images were acquired 20-30 min post i.v. injection of 10.7 ± 0.7 MBq of
4 [¹⁸F]FET (7,8,10,27). After each PET acquisition, the animal bed was transferred into the computed
5 tomography (CT) scanner (Inveon, Siemens Medical Solutions, U.S.) for anatomical co-registration with
6 the PET images using the image analysis software VINCI (Version: 4.19.0;
7 <http://www.nf.mpg.de/vinci3/>)(10,28).

8 A three step co-registration regimen was applied to assure exact image co-registration. First, PET and CT
9 images were co-registered employing three molecular sieve spheres, (Acros Organics, Geel, Belgium)
10 (two on the left side and one at the right side of the animal bed), rinsed in radiotracer solution and taped
11 onto the animal bed, being visible on CT and PET images. The automated “Landmark tool” was used to
12 superimpose CT images to PET images. The “Magic tool” was further applied to correct for minor
13 mismatches (Step 1, Suppl. Fig. 2). Secondly, CT images were co-registered to MR images using the
14 “Contour-“ and “Fusion-tool” provided by the VINCI software, assisting in delineating the skull and bone
15 of the mice. Several anatomic landmarks were used as quality measures of co-registration: the
16 paraflocculus region (MR) and its respective bone structure (CT), the temporomandibular joint region,
17 the sphenoidal bone, the bulbus olfactorius region, and the lambda region (thickening of the skull
18 dividing the visual cortex from midbrain and cerebellum on top of the inferior colliculus) (Step 2, **Suppl.**
19 **Fig. 2**). The reslicing parameters of the CT were transferred to the PET, resulting in fused PET-MR images
20 (Step 3, **Suppl. Fig. 2**). A thorough quality check of image registration in all 3 image planes was
21 performed after PET/CT/MR co-registration. The quality of co-registration was judged and confirmed by
22 three independent experts in the field (BZ, AW, and AHJ).

1 ***MRI studies***

2 MRI was performed with a 9.4 T small animal MR scanner (Bios-Spec 94/20; BrukerBioSpin MRI GmbH,
3 Germany). The system was operated using the software ParaVision 5.1. Anatomical 2D T2w rapid
4 acquisition with relaxation enhancement (RARE) brain images were obtained with a helium-cooled
5 Cryoprobe (BrukerBioSpin MRI GmbH) in three imaging planes (TR 3000-5500 ms, TE 50 ms, Rare factor
6 16, 6 averages, 14-28 contiguous slices, slice thickness 0.5 mm, field of view 20 mm², 256 matrix, in plane
7 resolution 78 μm², scan time 5-9 min, respectively). MRI was conducted for identification of glioma
8 location, and co-registration to PET images.

9 ***Data analysis***

10 Image data were analyzed using the in-house developed software MEDgical. Two different volumes of
11 interest (VOIs) were defined: (i) an elliptical control VOI covering the striatum (volume 6 mm³) was
12 drawn on the axial MR images and adjusted on the other imaging planes. This control VOI was re-used
13 for every mouse; (ii) a second glioma-covering elliptical VOI (volume 45 mm³) was drawn in the tumor
14 affected brain hemisphere, excluding the cerebellum. For quantification, a thresholding approach was
15 applied by multiplying the standard deviation of the control VOI by a factor of 2.5. The resulting counts
16 were added to the mean values of the control region. This was used as minimal threshold level of the
17 affected hemisphere and calculated for all three tracers individually (**Suppl. Fig. 3**). Tumor-to-background
18 ratios (T/B) were calculated between the glioma VOI (mean and max values) and the contralateral
19 control VOI (mean values). The control VOI constituted a standardized elliptical VOI placed over the left
20 striatum (**Suppl. Fig. 3**). For volumetric analysis, the resulting volumes of [¹⁸F]DPA-714 and [¹⁸F]BR-351
21 were compared to the clinical standard [¹⁸F]FET biomarker. First, the combined tracer volumes (union) of
22 [¹⁸F]DPA-714 with [¹⁸F]FET and [¹⁸F]BR-351 with [¹⁸F]FET were calculated using the MEDgical software
23 tool. Based on the union of the two tracer volumes the percentage of overlap was calculated. In a next
24 step, the exclusive [¹⁸F]DPA-714 and [¹⁸F]BR-351 uptake volumes were calculated by subtracting the

1 overlapping volumes of [¹⁸F]FET∩[¹⁸F]DPA-714 and [¹⁸F]FET∩[¹⁸F]BR-351 from the total [¹⁸F]DPA-714 or
2 [¹⁸F]BR-351 signal volume, respectively. The volumetric data were further analyzed comparing the two
3 different sequences of the multi-tracer approach for assessment of tumor growth effects on volumetry
4 **(Suppl. Fig. 4)**. The intra-rater test-retest reproducibility of co-registration was investigated by repeated
5 co-registration on two repeated co-registrations (coreg2 and coreg3) and compared to the initial
6 coregistration procedure (coreg1) in an exemplary set of $n=6$ mice for the relation of [¹⁸F]DPA-714 and
7 [¹⁸F]FET **(Suppl. Fig. 5)**.

8 ***Immunohistochemistry***

9 After the last imaging examination, mice were sacrificed and perfused with 0.9% NaCl and 4%
10 paraformaldehyde. Brains were fixed and embedded in paraffin. The sections were incubated over night
11 with antibodies for microglia (1:2000, goat anti Iba-1, ab107159, Abcam), MMP-9 (1:200, rabbit anti-
12 mouse MMP-9, ab38889, Abcam), and TSPO (1:250, rabbit, anti TSPO, NBP1-95674, Novus Biologicals,
13 Cambridge, United Kingdom). Immunohistochemistry for human and murine TSPO was done using the
14 Vector® M.O.M.™ Immunodetection Kit (Vector Laboratories, USA), the specific anti-human TSPO
15 antibody Mab 8D7(29) (1:500, generously provided by Dr. E. Bribes of Sanofi-Aventis, France) and the
16 specific anti-murine TSPO antibody (1:1000, generously provided by Dr. M. Higuchi, NIRS, Japan), in 0.5%
17 PBS-TWEEN with 5% BSA for 1 hour at room temperature, followed by incubation with Alexa Fluor 488-
18 conjugated anti-rabbit secondary antibody (1:800, A-21206, life technologies), or Alexa Fluor 555
19 conjugated anti-goat (1:800, A-21432, life technologies). Nuclei were stained with DAPI (0.2 µg/ml in
20 PBS, 6335.1, Roth, Karlsruhe, Germany). Conventional histology for TSPO and MMP-9 was performed
21 using biotinylated goat anti-rabbit (1:800, B21078, Life Technologies, Darmstadt, Germany), followed by
22 HRP-Streptavidin incubation (1:600, K1016, DAKO, Hamburg, Germany). The staining was visualized by
23 incubation with 3,3 Diaminobenzidine (D-5637, Sigma). Images were acquired with a combined
24 fluorescence-light microscope (Nikon Eclipse NI-E, Nikon, Japan).

1 ***Gel Zymography***

2 Mice were transcardially perfused with ice-cold PBS to get rid of excess blood for two min; brains were
3 immediately harvested afterwards. Subsequently, the tumor and the contralateral hemisphere were
4 dissected and snap frozen in liquid nitrogen. The samples were homogenized in a cooled micro
5 dismembrator (Sartorius, Göttingen, Germany). Tissue extracts were incubated for 10 min in lysis buffer
6 (50mM TRIS-HCl, 75 mM NaCl, 1 mM phenylmethylsulfonyl fluoride) and centrifuged (4°C, 20 min, 13000
7 rpm). An 8 % sodium dodecyl sulfate gel containing 0.1 % fish skin gelatin (Sigma Aldrich, St. Louis, MO,
8 USA) was prepared. 10 µg of total protein were loaded on the gel. Samples were stacked for 20 min at 60
9 V followed by 2 h at 125 V. The gel was washed in 2.5% Triton-X (30 min, RT), followed by incubation
10 over night with zymogram developing buffer (50 mM Tris-HCl, 0.2 M NaCl, 5 mM CaCl₂, 0.02% Brij 35, in
11 distilled and deionized water (AD)). The zymogram was stained (1 g Coomassie blue, 90 ml methanol, 20
12 ml acetic acid, 90 ml AD, 2h) and destained (50% methanol, 10% acetic acid, 40% AD, 15 min).

13 ***In situ zymography***

14 *N*=2 brains were harvested and 15 µm cryosections of the affected brains were sliced. After drying (30
15 min), slices were pre-incubated with 1 x buffer (5 min, EnzChek, life technologies, Carlsbad, USA), and
16 further incubated in a humidified chamber (8 h, 37°C) with 10x *in situ* zymography reaction buffer
17 (EnzChek), 7x MMP inhibitor (MMPi; cOmpete, Roche, Basel, Switzerland), fish skin gelatin (1 mg/ml),
18 and DQ gelatin (EnzChek) in AD. Slices were mounted in DAPI containing mounting medium (Vectashield,
19 H-1500, Vector Laboratories). As controls, slides were additionally incubated with 10 mM of the broad
20 spectrum MMP inhibitor 1,10-phenanthroline (EnzChek) in zymography reaction buffer to block MMP-
21 derived gelatinolytic activity(30).

22 ***Statistical analysis***

23 All statistical analyses were performed using Sigma Plot 13.0 software package (Systat Software, Erkrath,
24 Germany). All comparisons were tested for normality and variance homogeneity using the Sigma Plot

1 software. Differences in radiotracer uptake ratios between experimental and sham animals were tested
2 using a t-test, eventually followed by Mann-Whitney-U test on ranks. The inter-hemispheric difference in
3 the sham group was analyzed using paired t-tests. Differences in tracer signal volumes and intra-rater co-
4 reproducibility were tested using a one way repeated measures ANOVA (RM ANOVA), followed by
5 pairwise multiple comparisons using the Holm-Sidak method. Differences between the two groups of
6 different tracer sequences were tested by a one way ANOVA. Data are shown in Tukey box plots and bar
7 graphs. Significance levels were set at $p < 0.05$.

1

2 **Results**

3 *[¹⁸F]DPA-714, [¹⁸F]BR-351, and [¹⁸F]FET uptake is increased within and around the glioma.*

4 Multi-modality imaging in a mouse model of glioma for TSPO, MMPs and amino acid transport revealed
5 increased uptake of all three tracers within and around the tumor as compared to the healthy brain (**Fig.**
6 **1 A**). Tumor-to-background (Tmean/Bmean) (**Fig. 1 C**), as well as maximum tumor to mean background
7 (Tmax/Bmean) ratios (**Fig. 1 D**) of all three radiotracers were increased.

8 [¹⁸F]FET signal exceeded the hyperintense tumor area as depicted by T2w MRI. T/B uptake ratios for
9 [¹⁸F]FET were also increased compared to sham animals (Tmean/Bmean: 1.71 ± 0.21; Tmax/Bmean 2.87 ±
10 0.65, t-test, p<0.05 vs. Tmean/Bmean: 1.09 ± 0.11; Tmax/Bmean 1.57 ± 0.37) (**Fig. 1**). [¹⁸F]DPA-714
11 uptake was located within the tumor and adjacent brain parenchyma. Comparison of [¹⁸F]DPA-714 T/B
12 ratios with sham operated animals showed significantly increased uptake (Tmean/Bmean: 1.82 ± 0.21;
13 Tmax/Bmean 2.98 ± 0.73, t-test, p<0.05 vs. Tmean/Bmean: 1.11 ± 0.21; Tmax/Bmean 1.91 ± 0.34).

14 [¹⁸F]BR-351 uptake was restricted to the core of the tumor lesion. [¹⁸F]BR-351 uptake was increased
15 compared to sham animals (Tmean/Bmean: 1.83 ± 0.48; Tmax/Bmean 3.19 ± 1.19, t-test, p<0.05 vs.
16 Tmean/Bmean: 1.02 ± 0.11; Tmax/Bmean 2.09 ± 0.65). Within the experimental group, only one animal
17 showed no detectable [¹⁸F]BR-351 uptake after application of the thresholding.

18 For all three tracers, sham operated animals did not show any tracer uptake around the lesion (L) in
19 comparison with the contralateral hemisphere (B) (L/B_{DPA-714} 1.11 ± 0.21; L/B_{BR-351} 1.02 ± 0.11; L/B_{FET} 1.09
20 ± 0.11) (**Fig. 1 B, C**).

21

22 *Volumetric analysis and spatial comparison of tracer volumes*

23 Based on the applied thresholding, the resulting volumes of [¹⁸F]DPA-714 and [¹⁸F]BR-351 were
24 compared to the clinical standard [¹⁸F]FET biomarker, respectively (**Fig. 2 A**).

1 [¹⁸F]FET signal showed the largest mean number of voxel (493.3 ± 134.3 ; RM ANOVA; $p < 0.05$), compared
2 to [¹⁸F]DPA-714 (316.0 ± 105.4) and [¹⁸F]BR-351 (179.5 ± 131.5) (**Fig. 2 B**).

3 Comparison of the combination of both tracer volumes (union) of [¹⁸F]DPA-714 and [¹⁸F]FET uptake
4 volumes showed an overlap of 48.4 ± 11.1 % for both tracers.

5 In order to define volumes of exclusive tracer signal for [¹⁸F]DPA-714, the non-overlapping regions of
6 [¹⁸F]DPA-714 were further analyzed by subtracting the overlap of [¹⁸F]DPA-714 and [¹⁸F]FET from the
7 total [¹⁸F]DPA signal. 14 ± 14.5 % of the [¹⁸F]DPA-714 volumes were non-overlapping with [¹⁸F]FET. $45.1 \pm$
8 15.0 % of the [¹⁸F]FET volumes were non-overlapping with [¹⁸F]DPA-714 (**Fig. 2 C**).

9 The union of [¹⁸F]BR-351 derived signal together with the [¹⁸F]FET signal showed an overlap of $28.5 \pm$
10 18.0 %. Calculation of exclusive [¹⁸F]BR-351 signal indicated 11 ± 13.5 % of [¹⁸F]BR-351 signal as non-
11 overlapping with [¹⁸F]FET, whereas 68.8 ± 21.4 % of [¹⁸F]FET was non-overlapping with [¹⁸F]BR-351 (**Fig. 2**
12 **D**). Areas of exclusive [¹⁸F]DPA-714 and [¹⁸F]BR-351 were observed at the outer borders of the tumor
13 volume (**Fig. 2 A**). No significant effect on volumetric parameters obtained could be observed when
14 comparing the two different imaging sequences (**Suppl. Fig. 4**). Exemplary analysis of the volumetric
15 relation of [¹⁸F]DPA-714 and [¹⁸F]FET to address possible intra-rater variability did not reveal significant
16 changes, except for the percentage of [¹⁸F]DPA-714 signal for one co-registration (coreg 1 vs coreg 3:
17 11.0 ± 3.8 vs. 15.5 ± 5.5 ; RM ANOVA; $p < 0.05$) (**Suppl. Fig. 5**).

18

19 *Spatial agreement of radiotracers with histology*

20 Comparison of [¹⁸F]DPA-714 and [¹⁸F]BR-351 showed spatial agreement of PET volumes with histology
21 for TSPO and *in situ* zymography, respectively (**Fig. 3 A**). Higher magnification images highlight TSPO
22 reactivity arising from tumor cells (**Fig. 3 C**). However, cells of extra-tumoral tissue also displayed TSPO
23 immunoreactivity (**Fig. 3 C,D**). *In situ* zymography signal resulting from gelatinolytic activity revealed
24 MMP activity arising from the tumor tissue (**Fig. 3 E, F**). Sham operated animals display minor TSPO and
25 MMP-9 immunoreactivity along the injection tract (**Fig. 3 G-K**).

1 *Microglia as pivotal TSPO source in glioma*

2 Double immunohistochemistry of TSPO and MMP-9 with Iba-1 (red) indicated infiltrating glioma
3 associated microglia/macrophages (GAMs, red) as important source of TSPO and MMP expression,
4 respectively (**Fig. 4 A**). Specific human and murine antibodies against TSPO highlighted human TSPO,
5 hence glioma cells, as important source of TSPO. A fraction of tumor infiltrating cells of murine origin,
6 likely GAMs, also represent a significant source of TSPO (**Fig. 4 B**).

7

8 *Characterization of MMP activity*

9 *In situ* zymography depicted gelatinolytic activity (green) arising from tumor cells (blue). Co-incubation
10 with the MMP-specific inhibitor 1,10-phenanthroline inhibited gelatinolytic activity within the tumor,
11 suggesting MMP-specific gelatinolytic activity (**Fig. 5 A**). In addition, gel zymography revealed
12 upregulation of MMP-2 and MMP-9 (**Fig. 5 B**).

13

1

2 **Discussion**

3 This is the first *in vivo* study validating two new radiotracers targeting GAMs (TSPO) and MMP activation
4 in comparison to the clinically established marker for endothelial amino acid transport ($[^{18}\text{F}]\text{FET}$) in a
5 murine model of glioma. $[^{18}\text{F}]\text{DPA-714}$ uptake was increased in and around the MRI detectable glioma
6 area (~1.8-fold) mostly related to TSPO-expressing glioma cells. $[^{18}\text{F}]\text{BR-351}$ uptake was mostly increased
7 within the core of the tumor to a similar extent as DPA-714 (~1.8 fold). $[^{18}\text{F}]\text{FET}$ showed the largest area
8 with increased uptake (~1.7 fold). Immunohistochemistry and zymography indicated that GAMs may
9 serve as an important source for TSPO and MMP activity. A thresholding approach allowed to depict
10 tumor areas which may not be detected by a single tracer and/or MRI parameter alone. Combining the
11 three radiotracers provides *in vivo* insights into the heterogeneous tissue composition of gliomas with
12 regards to amino acid transport (FET), invasion (BR-351), neoangiogenesis (FET), and inflammation (DPA-
13 714). These biomarkers shall provide the basis for the development of dedicated therapies targeting
14 various tissue compartments within gliomas (e.g. GAMs).

15 *$[^{18}\text{F}]\text{DPA-714}$ imaging*

16 Previous studies in glioma bearing rats have highlighted $[^{18}\text{F}]\text{DPA-714}$ as a suitable imaging marker for
17 glioma-associated TSPO expression(7–9,12). In line with these studies, we show, in a murine model of
18 human glioma, a strong increase in $[^{18}\text{F}]\text{DPA-714}$ uptake in the tumor region compared to a contralateral
19 region 13 days after implantation of glioma cells. Approximately 50% of the sum of the TSPO signal and
20 the $[^{18}\text{F}]\text{FET}$ signal overlapped. 14% of $[^{18}\text{F}]\text{DPA-714}$ positive glioma tissue was exclusive for $[^{18}\text{F}]\text{DPA-714}$
21 and did not reveal $[^{18}\text{F}]\text{FET}$ uptake, whereas about half of the $[^{18}\text{F}]\text{FET}$ volumes was not seen by $[^{18}\text{F}]\text{DPA-}$
22 714. It should be noted, that the tumor growth as well as the intra-rater variability may partially have
23 influenced quantitative volumetric numbers. Nevertheless, our observations underline that unique areas
24 of $[^{18}\text{F}]\text{DPA-714}$ and $[^{18}\text{F}]\text{FET}$ are detectable within a comparable range, with no influence by the

1 sequence of image acquisition of the various radiotracers and only minor influence by test-retest
2 variability for the co-registration procedure. Exclusive areas of [¹⁸F]DPA-714 uptake in relation to [¹⁸F]FET
3 may have been underestimated due to the ongoing tumor growth over the period of image data
4 acquisition.

5 We specifically chose a sequential imaging approach over a randomized approach potentially reducing
6 bias, as this method yields comparable data with a relatively high sensitivity and relevance with regards
7 to clinical observations (31). In a comparable sequential imaging approach by Jensen and colleagues with
8 GBM patients the authors combined [¹²⁵I]CLINDE (TSPO) SPECT followed by [¹⁸F]FET and MRI and found
9 similar overlaps of CLINDE and FET (12-42%, *n*=3), whereas [¹²⁵I]CLINDE yielded more exclusive areas
10 than [¹⁸F]FET compared to MR.

11 The unique tissue areas at the tumor margins are of high interest, since other research suggested that
12 areas of increased TSPO expression might be related to sites of glioma infiltration (12,31) and the
13 combination of both might improve therapy decisions.

14 Sham operated animals displayed mild TSPO expression, which could not be confirmed by [¹⁸F]DPA-714
15 PET, indicative of a TSPO threshold level, as observed previously(10). Correlative histology for TSPO
16 revealed spatial agreement with [¹⁸F]DPA-714 radiotracer uptake. Detailed analysis of TSPO sources in
17 conjunction with the marker Iba-1 for microglia/macrophages indicated glioma cells as main source of
18 TSPO expression. In addition, GAMs also contributed to the signal whereas others have shown that
19 normal astrocytes did not seem to play a role(8). Immunohistochemistry with specific antibodies
20 distinguishing human and murine TSPO allowed to depict the different sources of TSPO, indicating that
21 GAMs contributed to the overall [¹⁸F]DPA-714 signal. However, it should be noted that the relative
22 contribution of GAMs to glioma TSPO expression may be small(12,32). Nevertheless GAMs are
23 particularly important, since a significant non-neoplastic part of gliomas consists of infiltrating GAMs(4).
24 They are known to acquire an alternatively activated phenotype and generate an anti-inflammatory,
25 tumor promoting environment, and therefore represent an attractive target for imaging-guided

1 therapy(4). GAM polarization is a highly versatile process *in vivo*(4). Thus, TSPO imaging might be a
2 potential way to monitor GAMs and may help to understand GAM function under normal and treatment
3 conditions.

4 In line with our data, several studies have shown increased TSPO expression in human glioma biopsies
5 (33–35), experimental glioma(7,8,12,36), but also in GAMs (8). This is of particular importance, since
6 TSPO has been proposed as a marker of glioma invasiveness(37) and elevated levels have been described
7 depending on the tumor grade using *in vivo* imaging(12).

8 Further research is needed to investigate the suitability of [¹⁸F]DPA-714 PET for non-invasive glioma
9 grading and investigation of treatment effects on tumor cells and GAMs. Treatment approaches
10 targeting GAMs in combination with anti-neoplastic therapies need further attention, since GAMs were
11 shown to be involved in escape from anti-angiogenic therapy and represent a potential biomarker for
12 treatment resistance(38).

13 [¹⁸F]BR-351 imaging

14 MMPs have been shown to be highly upregulated in glioma(39). Accordingly, we show spatial
15 colocalization of [¹⁸F]BR-351 with *in situ* zymography, as well as elevated levels of activated MMP-2 and
16 MMP-9 indicated by gel zymography, which are likely the major sources of [¹⁸F]BR-351 signal. The
17 elevated expression of the gelatinases, MMP-2 and to a lower extent MMP-9, is indicative of enhanced
18 intracerebral invasion and neoangiogenesis(40). Likewise to [¹⁸F]DPA-714, parts of the [¹⁸F]BR-351-
19 derived volume were not detected by [¹⁸F]FET and thus might hint towards regions of glioma
20 invasion(40). Remarkably, GAMs were found to express MMP-9 on the histological level. Interestingly,
21 this expression of MMP-9 can be attributed to MMP-2 expressing tumor cells, and is capable of
22 activating infiltrating immune cell derived gelatinases (39). Another link between GAMs and MMPs is the
23 activation of the latent form of MMP-2 through glioma-mediated membrane type-1 MMP expression by
24 microglial cells. This increased expression facilitates glioma invasion(15).

1 It will be interesting to see whether [¹⁸F]BR-351 can be used in other models with enhanced invasiveness
2 and/or neoangiogenesis (41), which are expected to express even higher levels of MMPs to distinguish
3 and characterize different growth patterns *in vivo*.

4 Besides the gelatinases, [¹⁸F]BR-351 can also bind to MMP-13. Although this work did not focus on MMP-
5 13, it should be noted that MMP-13 is also upregulated in glioma. Elevated levels of MMP-13 have been
6 linked to patient survival rates, and are reported as a marker for cancer stem cells(42,43). Further studies
7 may decipher the potential of [¹⁸F]BR-351 in imaging tumor stem cells in glioma.

8 [¹⁸F]FET imaging

9 [¹⁸F]FET is a valuable marker for active tumor volume with significantly higher sensitivity and specificity
10 in diagnosis of brain tumors over e.g. contrast enhanced MRI, [¹⁸F]FDG or [¹⁸F]FLT PET imaging (20,44–
11 46). In line with these findings, it has been reported that [¹⁸F]FET can be used as prognostic marker of
12 therapy response and it helps to distinguish active tumor volume from therapy-induced tissue alterations
13 or pseudoprogression(47).

14 However, there is an increasing debate to what extent the glioma-associated inflammatory response
15 affects [¹⁸F]FET uptake(48–50). Therefore, a combination of specific tracers targeting the
16 neuroinflammatory response, e.g. [¹⁸F]DPA-714, with [¹⁸F]FET and biopsies may provide a useful tool to
17 depict the relative contribution of inflammation to [¹⁸F]FET uptake. We report that [¹⁸F]DPA-714 and
18 [¹⁸F]FET volumes partially overlap (~50%), which might be an indication that inflammation may be an
19 important contributor to [¹⁸F]FET uptake in this model. The overlap may also represent a mixture of
20 cellular compartments (i.e., tumor cells and microglial cells).

21 In conclusion, multi-modal combined PET/ MR imaging has been shown to be superior in delineating
22 active tumor tissue with higher sensitivity and specificity(45,51). Multi-tracer and multi-sequence
23 PET/MRI opens a new avenue for the detailed non-invasive characterization of the heterogeneous
24 glioma tissue with respect to the disease-driving cellular compartments at various disease stages and

1 their response to therapy (vasculature-FET, tumor and inflammatory cells-DPA-714, and proteases-BR-
2 351). Especially, the non-invasive identification of GAMs may represent a fundamental step towards
3 immune cell directed therapies in combination with various targeted or non-targeted anti-neoplastic
4 agents(4). The detailed characterization of the tumor microenvironment before and after therapy **should**
5 improve the imaging-guided management of patients.

6 **Acknowledgements:**

7 The authors thank M Kattenbeck, S Köster, C Bätza, R Priebe, S Bouma, F Breuer, I Hoppe, C Möllmann,
8 and D Reinhardt for their excellent technical support, as well as Christian Döring for support on the
9 volumetric analyses.

10

1

2 **References**

3 1. Charles NA, Holland EC, Gilbertson R, Glass R, Kettenmann H. The brain tumor microenvironment.
4 Glia [Internet]. 2012 [cited 2016 May 30];60:502–14. Available from:
5 <http://www.ncbi.nlm.nih.gov/pubmed/22379614>

6 2. Pierce BL, Ballard-Barbash R, Bernstein L, Baumgartner RN, Neuhouser ML, Wener MH, et al.
7 Elevated biomarkers of inflammation are associated with reduced survival among breast cancer
8 patients. J Clin Oncol [Internet]. 2009 [cited 2016 May 30];27:3437–44. Available from:
9 <http://www.pubmedcentral.nih.gov/articlerender.fcgi?artid=2717751&tool=pmcentrez&rendertype=abstract>

11 3. Richter N, Wendt S, Georgieva PB, Hambardzumyan D, Nolte C, Kettenmann H. Glioma-associated
12 microglia and macrophages/monocytes display distinct electrophysiological properties and do not
13 communicate via gap junctions. Neurosci Lett [Internet]. 2014 [cited 2016 May 30];583:130–5.
14 Available from:
15 <http://www.pubmedcentral.nih.gov/articlerender.fcgi?artid=4274622&tool=pmcentrez&rendertype=abstract>

17 4. Hambardzumyan D, Gutmann DH, Kettenmann H. The role of microglia and macrophages in
18 glioma maintenance and progression. Nat Neurosci [Internet]. 2015 [cited 2016 Jan 4];19:20–7.
19 Available from: <http://www.ncbi.nlm.nih.gov/pubmed/26713745>

20 5. Miettinen H, Kononen J, Haapasalo H, Helén P, Sallinen P, Harjuntausta T, et al. Expression of
21 peripheral-type benzodiazepine receptor and diazepam binding inhibitor in human astrocytomas:
22 relationship to cell proliferation. Cancer Res [Internet]. 1995 [cited 2014 Jun 23];55:2691–5.
23 Available from: <http://cancerres.aacrjournals.org/content/55/12/2691.short>

- 1 6. Vlodavsky E, Soustiel JF. Immunohistochemical expression of peripheral benzodiazepine receptors
2 in human astrocytomas and its correlation with grade of malignancy, proliferation, apoptosis and
3 survival. *J Neurooncol* [Internet]. 2007 [cited 2014 Jun 23];81:1–7. Available from:
4 <http://www.ncbi.nlm.nih.gov/pubmed/16868661>
- 5 7. Awde AR, Boisgard R, Thézé B, Dubois A, Zheng J, Dollé F, et al. The translocator protein
6 radioligand 18F-DPA-714 monitors antitumor effect of erufosine in a rat 9L intracranial glioma
7 model. *J Nucl Med* [Internet]. 2013 [cited 2014 Feb 24];54:2125–31. Available from:
8 <http://www.ncbi.nlm.nih.gov/pubmed/24212976>
- 9 8. Winkeler A, Boisgard R, Awde AR, Dubois A, Thézé B, Zheng J, et al. The translocator protein
10 ligand [¹⁸F]DPA-714 images glioma and activated microglia in vivo. *Eur J Nucl Med Mol Imaging*
11 [Internet]. 2012;39:811–23. Available from: <http://www.ncbi.nlm.nih.gov/pubmed/22270507>
- 12 9. Tang D, Hight MR, McKinley ET, Fu A, Buck JR, Smith RA, et al. Quantitative preclinical imaging of
13 TSPO expression in glioma using N,N-diethyl-2-(2-(4-(2-18F-fluoroethoxy)phenyl)-5,7-
14 dimethylpyrazolo[1,5-a]pyrimidin-3-yl)acetamide. *J Nucl Med* [Internet]. 2012/01/19. 2012 [cited
15 2014 Jun 23];53:287–94. Available from: <http://www.ncbi.nlm.nih.gov/pubmed/22251555>
- 16 10. Zinnhardt B, Viel T, Wachsmuth L, Vrachimis A, Wagner S, Breyholz H-J, et al. Multimodal imaging
17 reveals temporal and spatial microglia and matrix metalloproteinase activity after experimental
18 stroke. *J Cereb Blood Flow Metab* [Internet]. International Society for Cerebral Blood Flow &
19 Metabolism, Inc.; 2015 [cited 2015 Jul 17]; Available from:
20 <http://dx.doi.org/10.1038/jcbfm.2015.149>
- 21 11. Jacobs AH, Tavitian B, consortium Inm. Noninvasive molecular imaging of neuroinflammation. *J*
22 *Cereb Blood Flow Metab* [Internet]. 2012;32:1393–415. Available from:
23 <http://www.ncbi.nlm.nih.gov/pubmed/22549622>

- 1 12. Buck JR, McKinley ET, Fu A, Abel TW, Thompson RC, Chambless L, et al. Preclinical TSPO Ligand
2 PET to Visualize Human Glioma Xenotransplants: A Preliminary Study. PLoS One [Internet]. 2015
3 [cited 2016 Jan 25];10:e0141659. Available from:
4 [http://www.pubmedcentral.nih.gov/articlerender.fcgi?artid=4627825&tool=pmcentrez&renderty
6 pe=abstract](http://www.pubmedcentral.nih.gov/articlerender.fcgi?artid=4627825&tool=pmcentrez&renderty
5 pe=abstract)
- 6 13. Lakka SS, Gondi CS, Rao JS. Proteases and Glioma Angiogenesis. Brain Pathol [Internet]. 2006
7 [cited 2016 Jan 11];15:327–41. Available from: [http://doi.wiley.com/10.1111/j.1750-
9 3639.2005.tb00118.x](http://doi.wiley.com/10.1111/j.1750-
8 3639.2005.tb00118.x)
- 9 14. Komatsu K, Nakanishi Y, Nemoto N, Hori T, Sawada T, Kobayashi M. Expression and quantitative
10 analysis of matrix metalloproteinase-2 and -9 in human gliomas. Brain Tumor Pathol [Internet].
11 2004 [cited 2014 Jun 23];21:105–12. Available from:
12 <http://www.ncbi.nlm.nih.gov/pubmed/15696970>
- 13 15. Markovic DS, Vinnakota K, Chirasani S, Synowitz M, Raguet H, Stock K, et al. Gliomas induce and
14 exploit microglial MT1-MMP expression for tumor expansion. Proc Natl Acad Sci U S A [Internet].
15 2009 [cited 2014 Aug 13];106:12530–5. Available from:
16 [http://www.pubmedcentral.nih.gov/articlerender.fcgi?artid=2718387&tool=pmcentrez&renderty
18 pe=abstract](http://www.pubmedcentral.nih.gov/articlerender.fcgi?artid=2718387&tool=pmcentrez&renderty
17 pe=abstract)
- 18 16. Markovic DS, Glass R, Synowitz M, Rooijen N van, Kettenmann H. Microglia stimulate the
19 invasiveness of glioma cells by increasing the activity of metalloprotease-2. J Neuropathol Exp
20 Neurol [Internet]. 2005 [cited 2014 Aug 13];64:754–62. Available from:
21 <http://www.ncbi.nlm.nih.gov/pubmed/16141784>
- 22 17. Lin H-C, Song T-Y, Hu M-L. S-Adenosylhomocysteine promotes the invasion of C6 glioma cells via
23 increased secretion of matrix metalloproteinase-2 in murine microglial BV2 cells. Toxicol Sci

- 1 [Internet]. 2009 [cited 2016 May 30];112:322–30. Available from:
2 <http://www.ncbi.nlm.nih.gov/pubmed/19770485>
- 3 18. McQuibban GA, Gong JH, Wong JP, Wallace JL, Clark-Lewis I, Overall CM. Matrix
4 metalloproteinase processing of monocyte chemoattractant proteins generates CC chemokine
5 receptor antagonists with anti-inflammatory properties in vivo. *Blood* [Internet]. 2002/08/01.
6 2002;100:1160–7. Available from: <http://www.ncbi.nlm.nih.gov/pubmed/12149192>
- 7 19. Wagner S, Faust A, Breyholz HJ, Schober O, Schafers M, Kopka K. The MMP inhibitor (R)-2-(N-
8 benzyl-4-(2-[18F]fluoroethoxy)phenylsulphonamido)-N-hydroxy-3-methylbuta namide: Improved
9 precursor synthesis and fully automated radiosynthesis. *Appl Radiat Isot* [Internet]. 2011/03/19.
10 2011;69:862–8. Available from: <http://www.ncbi.nlm.nih.gov/pubmed/21414792>
- 11 20. Hutterer M, Nowosielski M, Putzer D, Jansen NL, Seiz M, Schocke M, et al. [18F]-fluoro-ethyl-L-
12 tyrosine PET: a valuable diagnostic tool in neuro-oncology, but not all that glitters is glioma.
13 *Neuro Oncol* [Internet]. 2013 [cited 2014 Jul 1];15:341–51. Available from:
14 [http://www.pubmedcentral.nih.gov/articlerender.fcgi?artid=3578481&tool=pmcentrez&rendertype](http://www.pubmedcentral.nih.gov/articlerender.fcgi?artid=3578481&tool=pmcentrez&rendertype=abstract)
15 [pe=abstract](http://www.pubmedcentral.nih.gov/articlerender.fcgi?artid=3578481&tool=pmcentrez&rendertype=abstract)
- 16 21. Kilkenny C, Browne WJ, Cuthill IC, Emerson M, Altman DG. The ARRIVE Guidelines Animal
17 Research: Reporting of In Vivo Experiments. 2013;
- 18 22. Nishikawa R, Ji XD, Harmon RC, Lazar CS, Gill GN, Cavenee WK, et al. A mutant epidermal growth
19 factor receptor common in human glioma confers enhanced tumorigenicity. *Proc Natl Acad Sci U*
20 *S A* [Internet]. 1994 [cited 2014 Aug 11];91:7727–31. Available from:
21 [http://www.pubmedcentral.nih.gov/articlerender.fcgi?artid=44475&tool=pmcentrez&rendertype](http://www.pubmedcentral.nih.gov/articlerender.fcgi?artid=44475&tool=pmcentrez&rendertype=abstract)
22 [=abstract](http://www.pubmedcentral.nih.gov/articlerender.fcgi?artid=44475&tool=pmcentrez&rendertype=abstract)
- 23 23. Abe T, Wakimoto H, Bookstein R, Maneval DC, Chiocca EA, Basilion JP. Intra-arterial delivery of

- 1 p53-containing adenoviral vector into experimental brain tumors. *Cancer Gene Ther* [Internet].
2 2002 [cited 2014 Aug 11];9:228–35. Available from:
3 <http://www.ncbi.nlm.nih.gov/pubmed/11896438>
- 4 24. James ML, Fulton RR, Vercoullie J, Henderson DJ, Garreau L, Chalon S, et al. DPA-714, a new
5 translocator protein-specific ligand: synthesis, radiofluorination, and pharmacologic
6 characterization. *J Nucl Med* [Internet]. 2008/04/17. 2008;49:814–22. Available from:
7 <http://www.ncbi.nlm.nih.gov/pubmed/18413395>
- 8 25. Pauleit D, Stoffels G, Schaden W, Hamacher K, Bauer D, Tellmann L, et al. PET with O-(2-18F-
9 Fluoroethyl)-L-Tyrosine in peripheral tumors: first clinical results. *J Nucl Med* [Internet]. 2005
10 [cited 2014 Sep 15];46:411–6. Available from: <http://www.ncbi.nlm.nih.gov/pubmed/15750152>
- 11 26. Schäfers KP, Reader AJ, Kriens M, Knoess C, Schober O, Schäfers M. Performance evaluation of
12 the 32-module quadHIDAC small-animal PET scanner. *J Nucl Med* [Internet]. 2005;46:996–1004.
13 Available from: <http://www.ncbi.nlm.nih.gov/pubmed/15937311>
- 14 27. Nedergaard MK, Kristoffersen K, Michaelsen SR, Madsen J, Poulsen HS, Stockhausen M-T, et al.
15 The use of longitudinal 18F-FET MicroPET imaging to evaluate response to irinotecan in
16 orthotopic human glioblastoma multiforme xenografts. *PLoS One* [Internet]. Public Library of
17 Science; 2014 [cited 2016 Nov 11];9:e100009. Available from:
18 <http://www.ncbi.nlm.nih.gov/pubmed/24918622>
- 19 28. Vollmar SCJ, Sue M, Klein J, Jacobs AH, Herholz K. VINCI-Volume Imaging in Neurological
20 Research, Co-Registration and ROIs Forschung und wissenschaftliches Rechnen 2003. Göttingen
21 Gesellschaft für wissenschaftliche Datenverarbeitung. 2004;115–31.
- 22 29. Bribes E, Carrière D, Goubet C, Galiègue S, Casellas P, Simony-Lafontaine J. Immunohistochemical
23 assessment of the peripheral benzodiazepine receptor in human tissues. *J Histochem Cytochem*

- 1 [Internet]. 2004 [cited 2016 Jun 13];52:19–28. Available from:
2 <http://www.ncbi.nlm.nih.gov/pubmed/14688214>
- 3 30. Bremer C, Tung C-H, Weissleder R. In vivo molecular target assessment of matrix
4 metalloproteinase inhibition. *Nat Med* [Internet]. Nature Publishing Group; 2001 [cited 2016 Nov
5 9];7:743–8. Available from: <http://www.nature.com/doi/10.1038/89126>
- 6 31. Jensen P, Feng L, Law I, Svarer C, Knudsen GM, Mikkelsen JD, et al. TSPO Imaging in Glioblastoma
7 Multiforme: A Direct Comparison Between 123I-CLINDE SPECT, 18F-FET PET, and Gadolinium-
8 Enhanced MR Imaging. *J Nucl Med* [Internet]. 2015 [cited 2016 Jan 11];56:1386–90. Available
9 from: <http://jnm.snmjournals.org/content/56/9/1386.full>
- 10 32. Janczar K, Su Z, Raccagni I, Anfosso A, Kelly C, Durrenberger PF, et al. The 18-kDa mitochondrial
11 translocator protein in gliomas: from the bench to bedside. *Biochem Soc Trans* [Internet]. 2015
12 [cited 2016 Jun 14];43:579–85. Available from: <http://www.ncbi.nlm.nih.gov/pubmed/26551696>
- 13 33. Black KL, Ikezaki K, Santori E, Becker DP, Vinters H V. Specific high-affinity binding of peripheral
14 benzodiazepine receptor ligands to brain tumors in rat and man. *Cancer* [Internet]. 1990 [cited
15 2014 Aug 14];65:93–7. Available from: <http://www.ncbi.nlm.nih.gov/pubmed/2152852>
- 16 34. Junck L, Olson JM, Ciliax BJ, Koeppe RA, Watkins GL, Jewett DM, et al. PET imaging of human
17 gliomas with ligands for the peripheral benzodiazepine binding site. *Ann Neurol* [Internet]. 1989
18 [cited 2014 Aug 14];26:752–8. Available from: <http://www.ncbi.nlm.nih.gov/pubmed/2557794>
- 19 35. Olson JM, Junck L, Young AB, Penney JB, Mancini WR. Isoquinoline and peripheral-type
20 benzodiazepine binding in gliomas: implications for diagnostic imaging. *Cancer Res* [Internet].
21 1988 [cited 2014 Aug 14];48:5837–41. Available from:
22 <http://www.ncbi.nlm.nih.gov/pubmed/3262414>

- 1 36. Buck JR, McKinley ET, Hight MR, Fu A, Tang D, Smith RA, et al. Quantitative, preclinical PET of
2 translocator protein expression in glioma using 18F-N-fluoroacetyl-N-(2,5-dimethoxybenzyl)-2-
3 phenoxyaniline. *J Nucl Med* [Internet]. 2011 [cited 2014 Aug 14];52:107–14. Available from:
4 <http://www.pubmedcentral.nih.gov/articlerender.fcgi?artid=3027353&tool=pmcentrez&rendertype=abstract>
5
- 6 37. Veenman L, Levin E, Weisinger G, Leschiner S, Spanier I, Snyder SH, et al. Peripheral-type
7 benzodiazepine receptor density and in vitro tumorigenicity of glioma cell lines. *Biochem*
8 *Pharmacol* [Internet]. 2004 [cited 2014 Sep 16];68:689–98. Available from:
9 <http://www.ncbi.nlm.nih.gov/pubmed/15276076>
- 10 38. Lu-Emerson C, Snuderl M, Kirkpatrick ND, Goveia J, Davidson C, Huang Y, et al. Increase in tumor-
11 associated macrophages after antiangiogenic therapy is associated with poor survival among
12 patients with recurrent glioblastoma. *Neuro Oncol* [Internet]. 2013 [cited 2016 May 31];15:1079–
13 87. Available from:
14 <http://www.pubmedcentral.nih.gov/articlerender.fcgi?artid=3714160&tool=pmcentrez&rendertype=abstract>
15
- 16 39. Koutroulis I, Zarros A, Theocharis S. The role of matrix metalloproteinases in the pathophysiology
17 and progression of human nervous system malignancies: a chance for the development of
18 targeted therapeutic approaches? *Expert Opin Ther Targets* [Internet]. 2008 [cited 2014 Aug
19 7];12:1577–86. Available from: <http://www.ncbi.nlm.nih.gov/pubmed/19007324>
- 20 40. Forsyth PA, Laing TD, Gibson AW, Rewcastle NB, Brasher P, Sutherland G, et al. High levels of
21 gelatinase-B and active gelatinase-A in metastatic glioblastoma. *J Neurooncol* [Internet]. 1998
22 [cited 2014 Aug 7];36:21–9. Available from: <http://www.ncbi.nlm.nih.gov/pubmed/9525822>
- 23 41. Viel T, Schelhaas S, Wagner S, Wachsmuth L, Schwegmann K, Kuhlmann M, et al. Early assessment

- 1 of the efficacy of temozolomide chemotherapy in experimental glioblastoma using [18F]FLT-PET
2 imaging. PLoS One [Internet]. 2013 [cited 2014 Jun 23];8:e67911. Available from:
3 <http://www.pubmedcentral.nih.gov/articlerender.fcgi?artid=3701682&tool=pmcentrez&rendertype=abstract>
4
- 5 42. Inoue A, Takahashi H, Harada H, Kohno S, Ohue S, Kobayashi K, et al. Cancer stem-like cells of
6 glioblastoma characteristically express MMP-13 and display highly invasive activity. Int J Oncol
7 [Internet]. 2010 [cited 2014 Sep 17];37:1121–31. Available from:
8 <http://www.ncbi.nlm.nih.gov/pubmed/20878060>
- 9 43. Okoye-Okafor UC, Bartholdy B, Cartier J, Gao EN, Pietrak B, Rendina AR, et al. New IDH1 mutant
10 inhibitors for treatment of acute myeloid leukemia. Nat Chem Biol [Internet]. 2015 [cited 2016
11 Jan 21];11:878–86. Available from: <http://www.ncbi.nlm.nih.gov/pubmed/26436839>
- 12 44. Pauleit D, Floeth F, Hamacher K, Riemenschneider MJ, Reifenberger G, Müller H-W, et al. O-(2-
13 [18F]fluoroethyl)-L-tyrosine PET combined with MRI improves the diagnostic assessment of
14 cerebral gliomas. Brain [Internet]. 2005 [cited 2014 Jul 1];128:678–87. Available from:
15 <http://www.ncbi.nlm.nih.gov/pubmed/15689365>
- 16 45. Nowosielski M, Difranco MD, Putzer D, Seiz M, Recheis W, Jacobs AH, et al. An Intra-Individual
17 Comparison of MRI, [18F]-FET and [18F]-FLT PET in Patients with High-Grade Gliomas. PLoS One
18 [Internet]. 2014 [cited 2014 Jul 1];9:e95830. Available from:
19 <http://www.pubmedcentral.nih.gov/articlerender.fcgi?artid=3997484&tool=pmcentrez&rendertype=abstract>
20
- 21 46. Galldiks N, Langen K-J, Holy R, Pinkawa M, Stoffels G, Nolte KW, et al. Assessment of treatment
22 response in patients with glioblastoma using O-(2-18F-fluoroethyl)-L-tyrosine PET in comparison
23 to MRI. J Nucl Med [Internet]. 2012 [cited 2014 Jul 1];53:1048–57. Available from:

- 1 <http://www.ncbi.nlm.nih.gov/pubmed/22645298>
- 2 47. Hutterer M, Nowosielski M, Putzer D, Waitz D, Tinkhauser G, Kostron H, et al. O-(2-18F-
- 3 fluoroethyl)-L-tyrosine PET predicts failure of antiangiogenic treatment in patients with recurrent
- 4 high-grade glioma. *J Nucl Med* [Internet]. 2011 [cited 2014 Sep 15];52:856–64. Available from:
- 5 <http://www.ncbi.nlm.nih.gov/pubmed/21622893>
- 6 48. Hutterer M, Nowosielski M, Putzer D, Fougère C la, Virgolini IJ, Jacobs AH, et al. Response to
- 7 “reply to [18F]-fluoro-ethyl-L-tyrosine PET: a valuable diagnostic tool in neuro-oncology, but not
- 8 all that glitters is glioma” by Hutterer et al. *Neuro Oncol* [Internet]. 2013 [cited 2014 Sep
- 9 15];15:814–5. Available from:
- 10 <http://www.pubmedcentral.nih.gov/articlerender.fcgi?artid=3688024&tool=pmcentrez&renderty>
- 11 [pe=abstract](http://www.pubmedcentral.nih.gov/articlerender.fcgi?artid=3688024&tool=pmcentrez&renderty)
- 12 49. Langen K-J, Galldiks N. Reply to “[18F]-fluoro-ethyl-L-tyrosine PET: a valuable diagnostic tool in
- 13 neuro-oncology, but not all that glitters is glioma” by Hutterer et al. *Neuro Oncol* [Internet]. 2013
- 14 [cited 2014 Sep 15];15:816–7. Available from:
- 15 <http://www.pubmedcentral.nih.gov/articlerender.fcgi?artid=3688021&tool=pmcentrez&renderty>
- 16 [pe=abstract](http://www.pubmedcentral.nih.gov/articlerender.fcgi?artid=3688021&tool=pmcentrez&renderty)
- 17 50. Piroth MD, Prasath J, Willuweit A, Stoffels G, Sellhaus B, van Osterhout A, et al. Uptake of O-(2-
- 18 [18F]fluoroethyl)-L-tyrosine in reactive astrocytosis in the vicinity of cerebral gliomas. *Nucl Med*
- 19 *Biol* [Internet]. 2013 [cited 2014 Jul 1];40:795–800. Available from:
- 20 <http://www.ncbi.nlm.nih.gov/pubmed/23769262>
- 21 51. Dhermain FG, Hau P, Lanfermann H, Jacobs AH, van den Bent MJ. Advanced MRI and PET imaging
- 22 for assessment of treatment response in patients with gliomas. *Lancet Neurol* [Internet]. 2010
- 23 [cited 2014 Aug 14];9:906–20. Available from:

2 **Figure Legends:**

3
4 **Figure 1:** Multi-tracer approach to characterize the glioma microenvironment. (A) PET images for [¹⁸F]FET
5 [¹⁸F]DPA-714, and [¹⁸F]BR-351 (left, top to bottom) and their fusion with T2w MRI (right, top to bottom).
6 The dotted line indicates the tumor area depicted by MRI and was transferred to PET images. (B)
7 Representative fusion images of sham operated animals. (C) Tmean/Bmean ratios showed significantly
8 increased uptake for [¹⁸F]DPA-714, [¹⁸F]BR-351 and [¹⁸F]FET. (D) Investigation of Tmax/Bmean ratios.

9
10 **Figure 2:** Volumetric analysis of PET tracer uptake. (A) Illustration of tracer volumes fused on T2wMRI.
11 (B) [¹⁸F]FET signal volume after thresholding showed the biggest number of voxel, compared to [¹⁸F]DPA-
12 714 and [¹⁸F]BR-351. (C+D) Comparison of the overlap of the combined tracer volumes, as well as unique
13 areas of tracer uptake.

14
15 **Figure 3:** Spatial comparison of [¹⁸F]DPA-714 and [¹⁸F]BR-351 with histology and *in situ* zymography. (A)
16 Comparison of PET data with histology for TSPO and *in situ* zymography revealed good spatial agreement
17 with the respective PET signal. (B-F) TSPO and MMP signal coming from the tumor cells and surrounding
18 tissue (TSPO, arrows). (G-K) Sham operated animals/brains displayed no tracer uptake. Slight
19 immunoreactivity was observed for TSPO along the injection tract (Scale bar: 1000 μm overview scans;
20 100/10 μm higher magnification images).

21
22 **Figure 4:** Role of GAMs for TSPO/MMP signal. (A) Double immunohistochemistry of Iba-1 (red) with TSPO
23 (green, left) and MMP-9 (green, right) showed Iba-1 expressing cells as source of TSPO and MMP-9 (Scale
24 bar 50 μm). (B) Comparison of human TSPO (red) and murine TSPO (green) identified tumor cells as
25 major source of TSPO. Infiltrating murine cells also contributed to the TSPO signal (Scale bar 200 μm).

1
2 **Figure 5:** Determining MMP activity in gliomas. (A) *In situ* zymography confirmed gelatinolytic activity
3 (green) resulting from the tumor region. Co-incubation with 1,10-phenanthroline inhibited gelatinolytic
4 activity (Scale bar 500 μm). (B) Gel zymography revealed an increase of activated MMP-2 and MMP-9 in
5 the tumor region compared to the contralateral side.

6

7

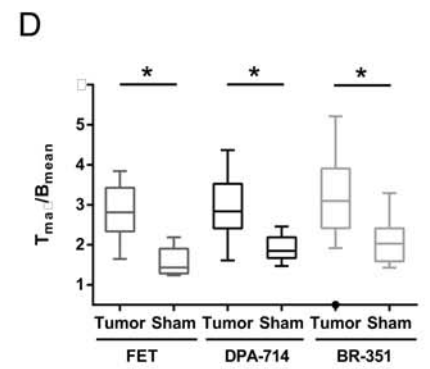
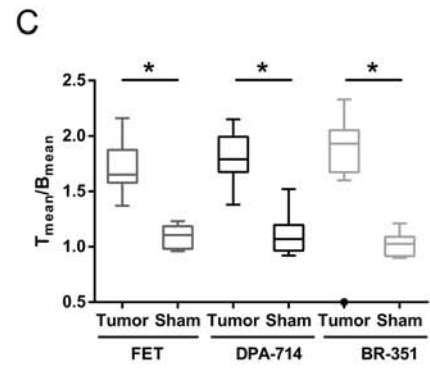
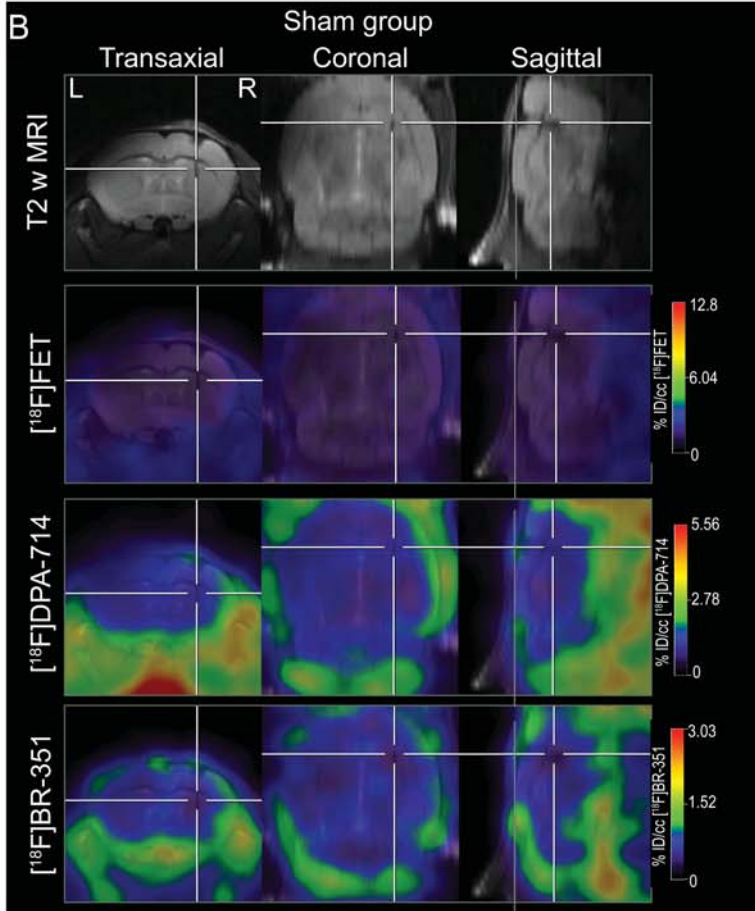
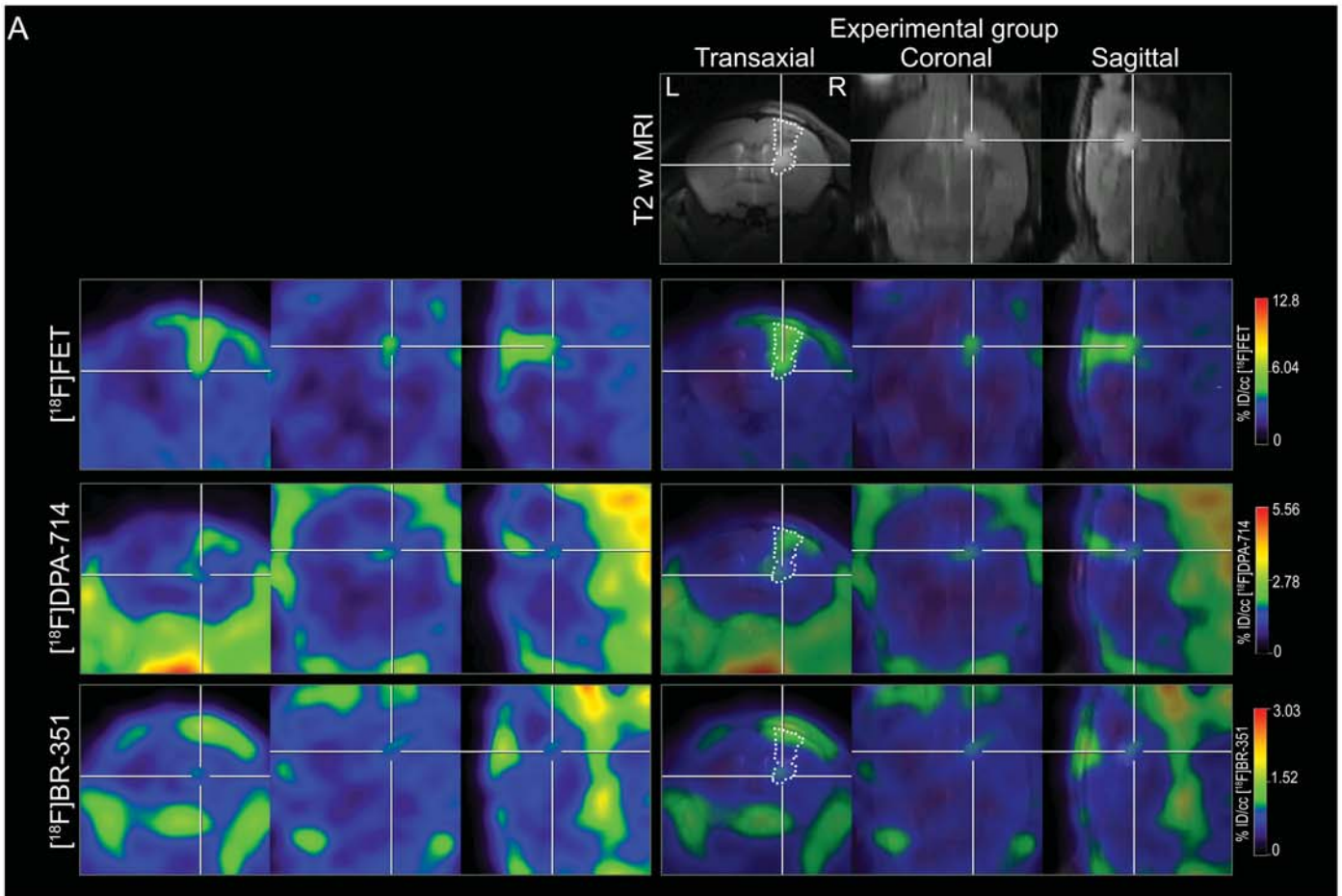


Figure 1

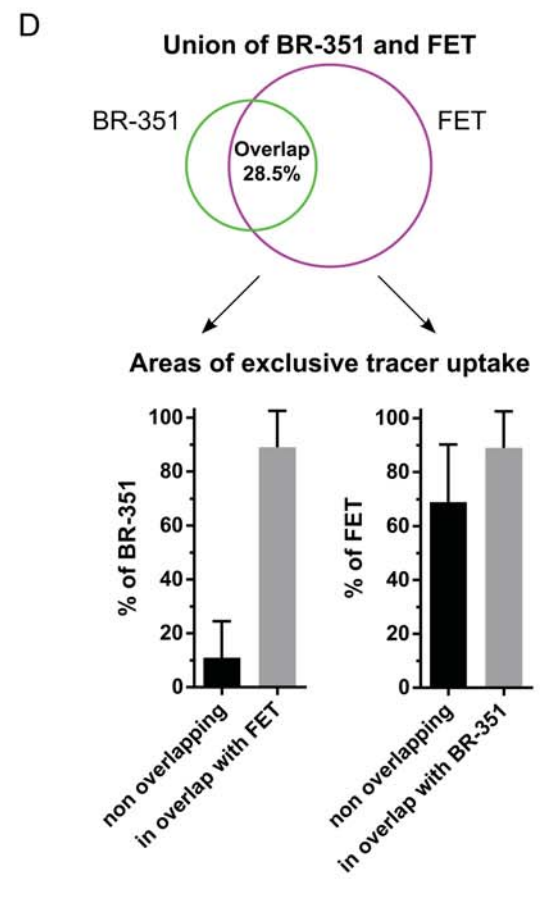
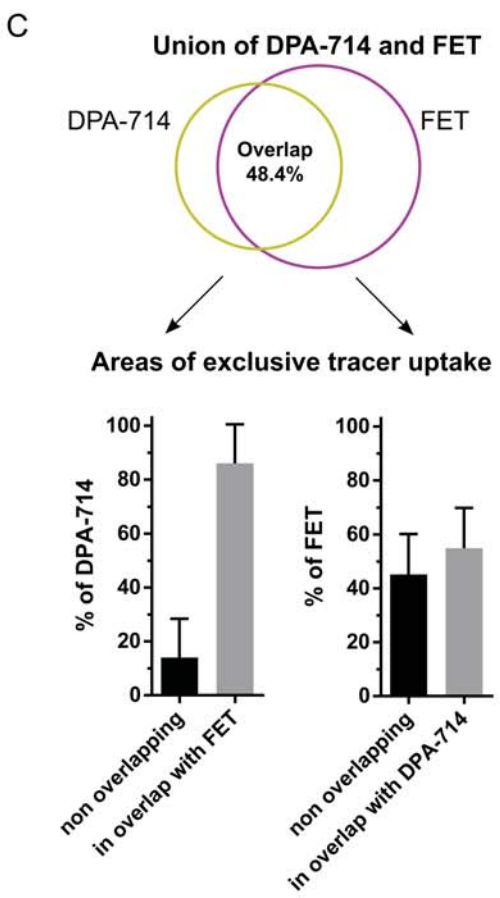
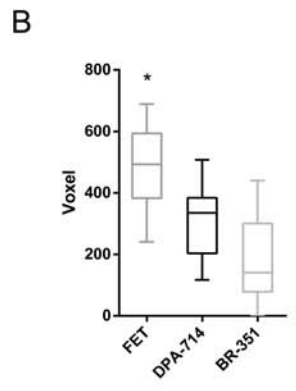
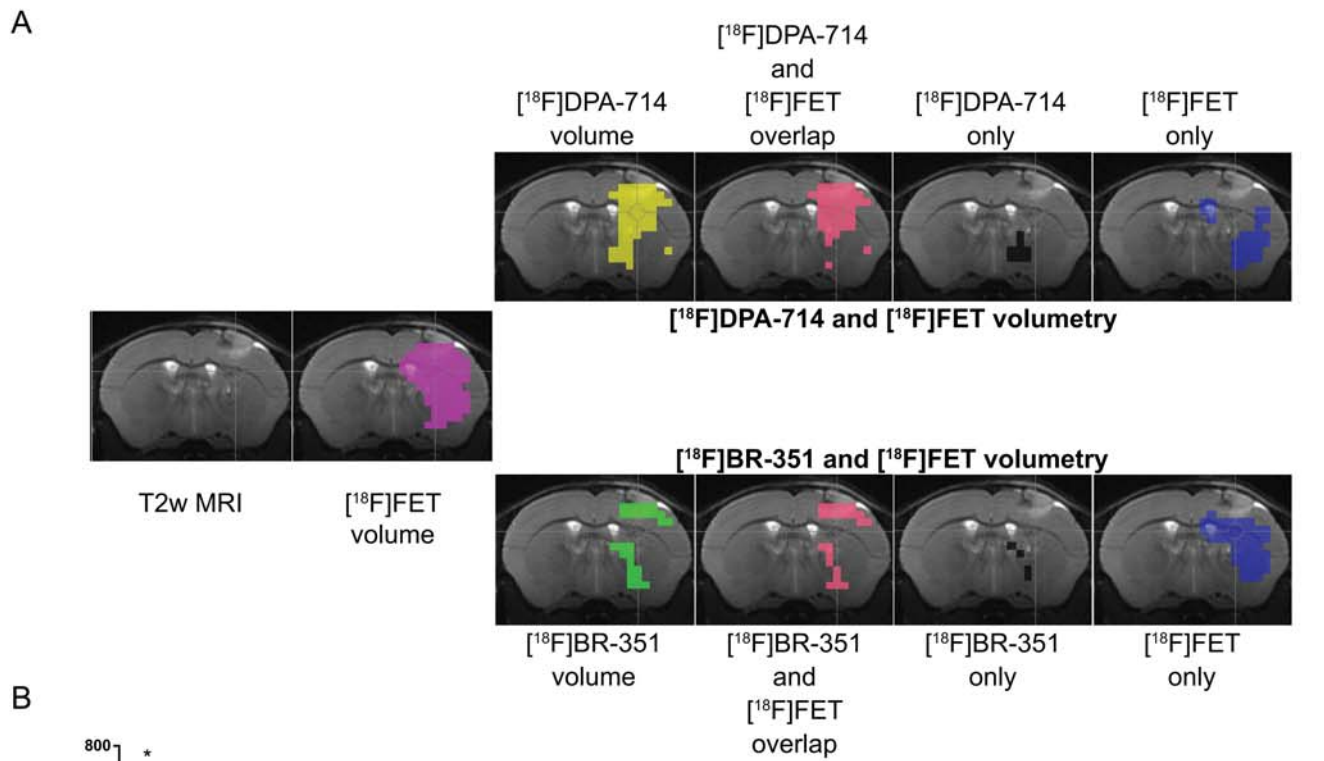


Figure 2

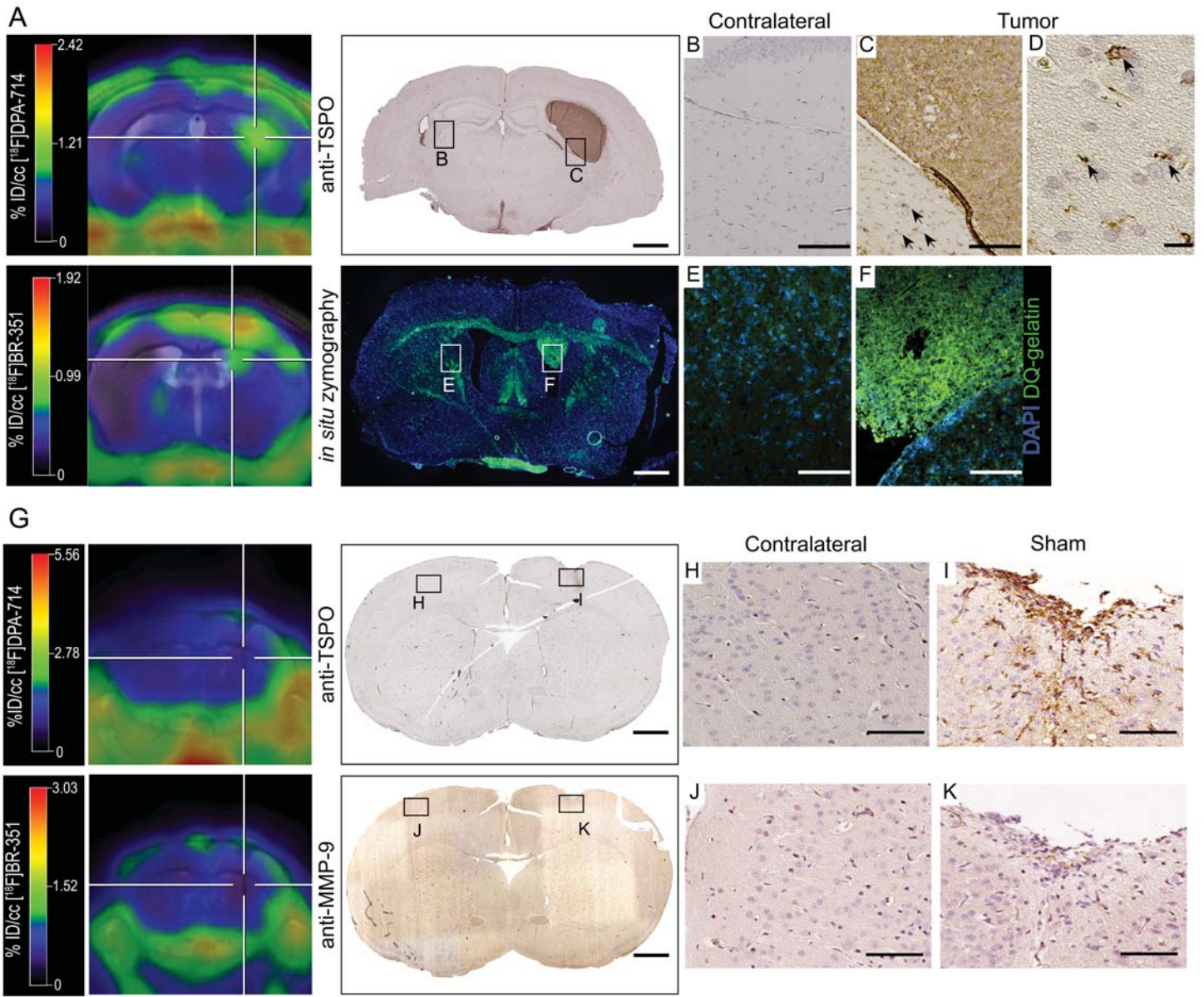
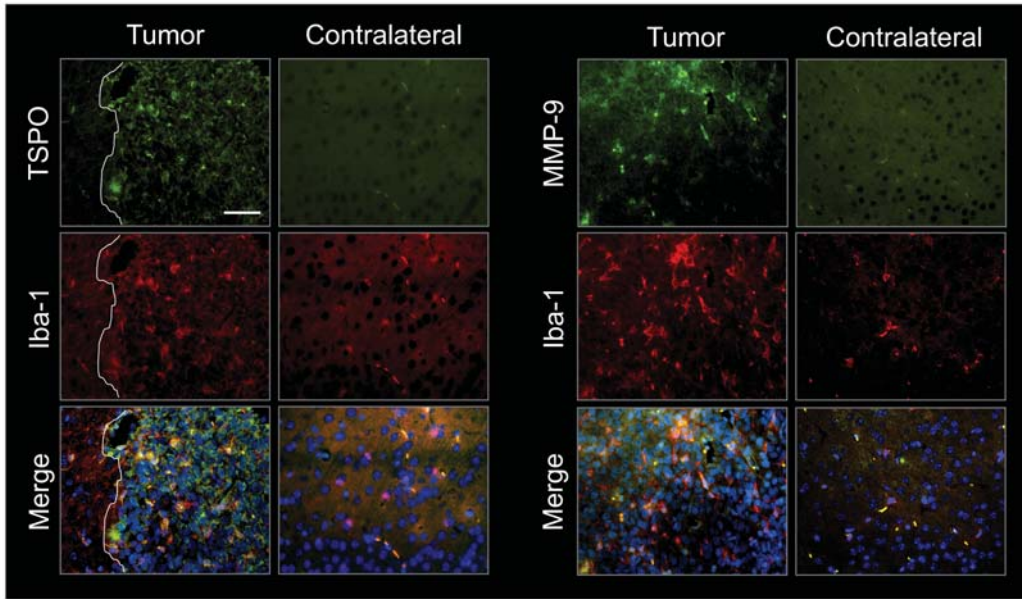


Figure 3

A



B

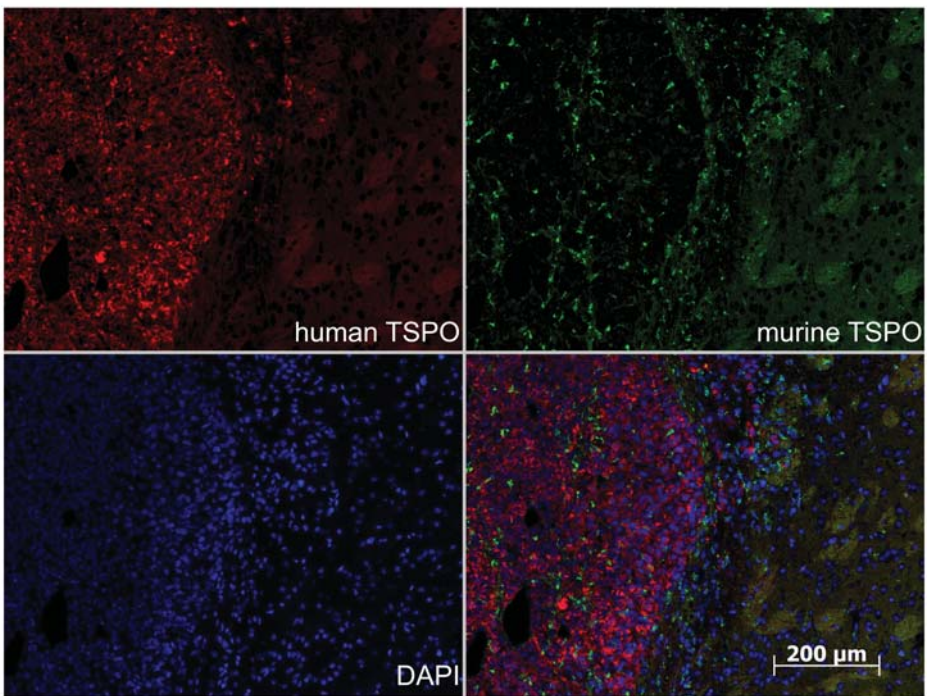


Figure 4

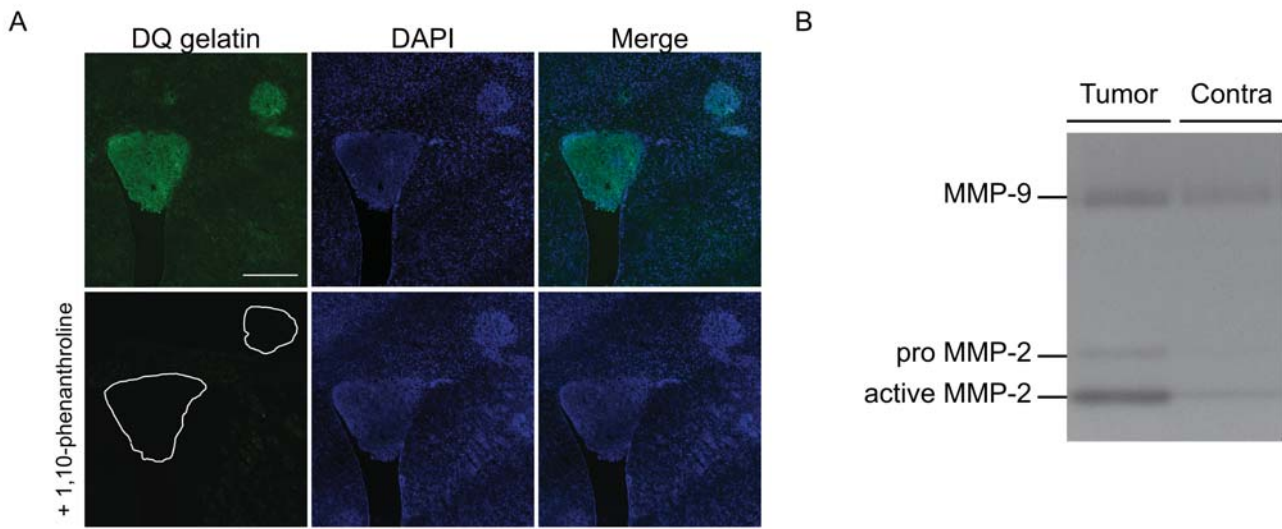


Figure 5